Supplement of The Cryosphere, 19, 267–282, 2025
https://doi.org/10.5194/tc-19-267-2025-supplement

The Cryosphere Open Access EGU

Supplement of

Creep enhancement and sliding in a temperate, hard-bedded alpine glacier

Juan-Pedro Roldán-Blasco et al.

Correspondence to: Adrien Gilbert (adrien.gilbert@univ-grenoble-alpes.fr)

Contents

S1. Recorded tilt timeseries

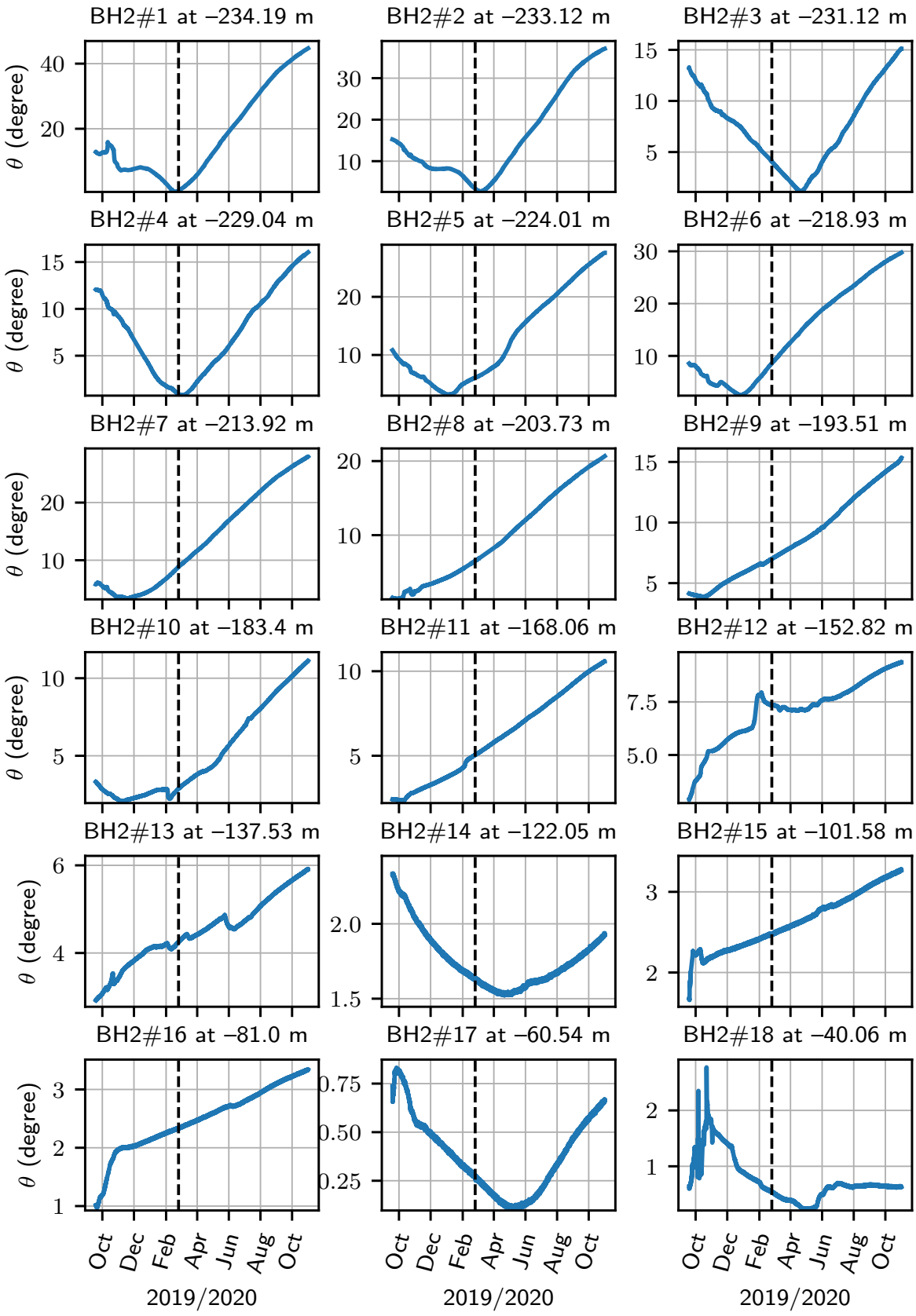

Figure S1: Temporal evolution of the tilt θ at each inclinometer #1-18 of borehole BH2. The depth of each sensor is indicated in the title of each panel.

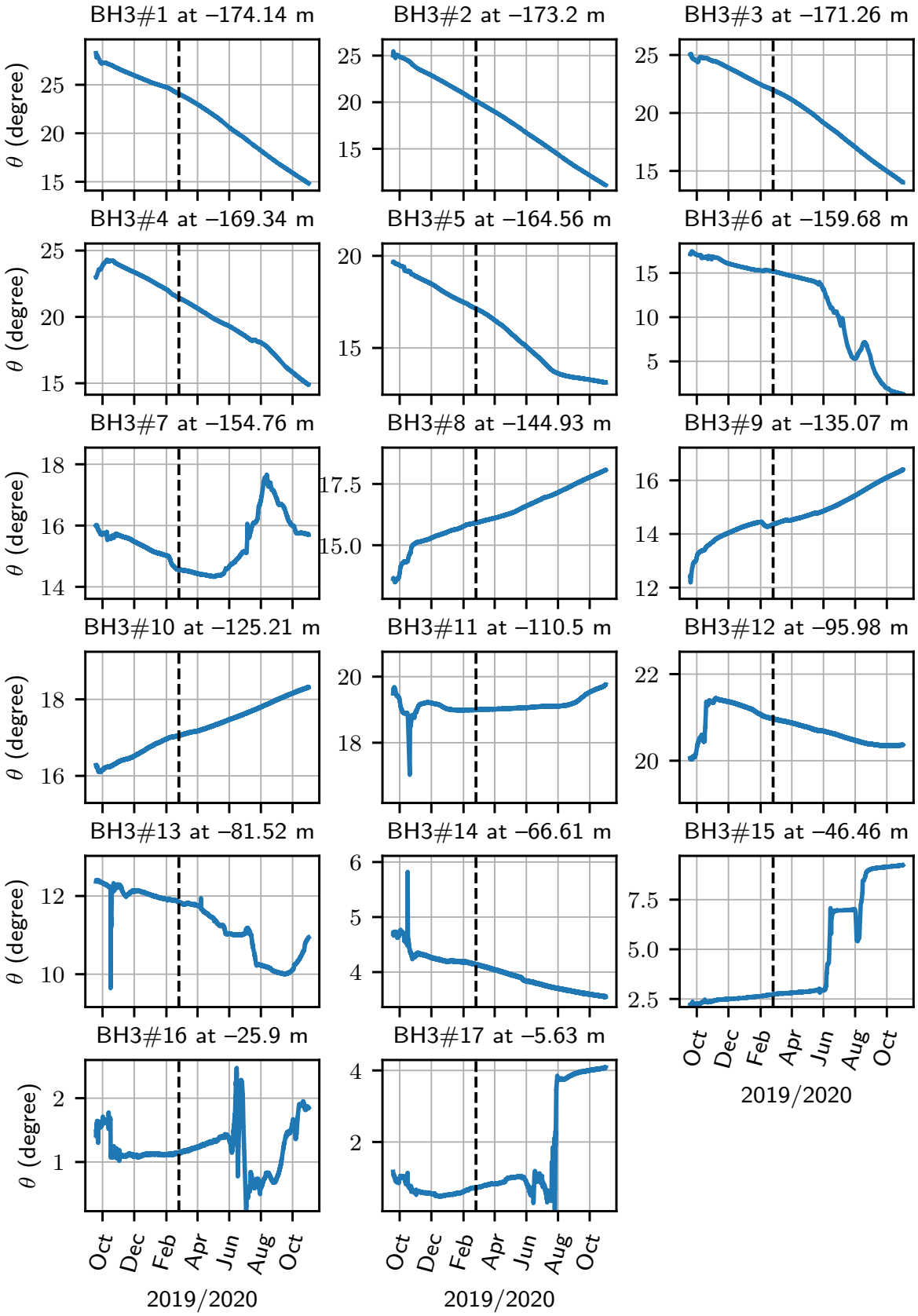

Figure S2: Same as Figure S1 but for inclinometers #1 to #17 of BH3

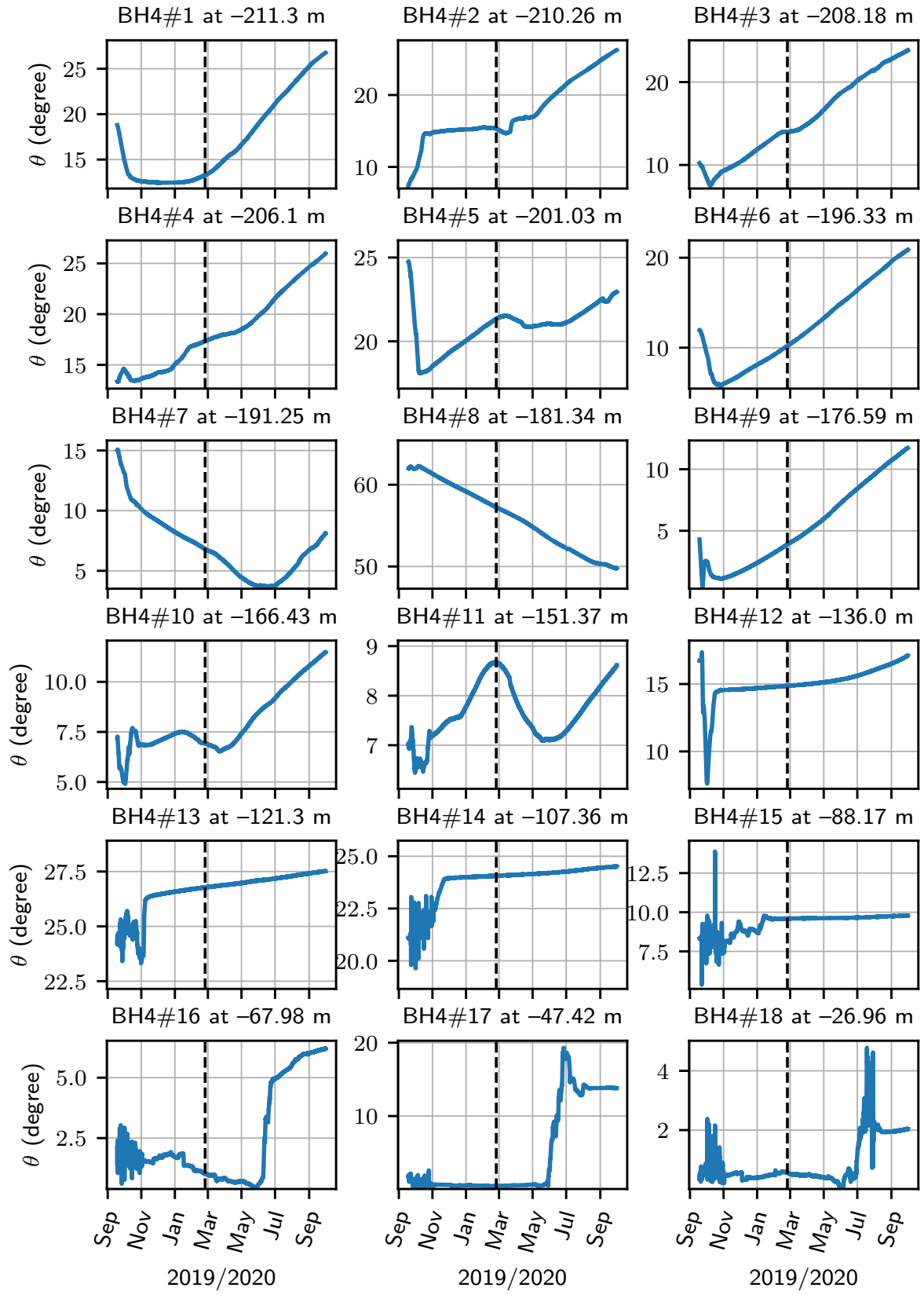

Figure S3: Same as Figure S1 but for inclinometers #1 to #18 of BH4

S2. Analysis using the Keller and Blatter (2012) model

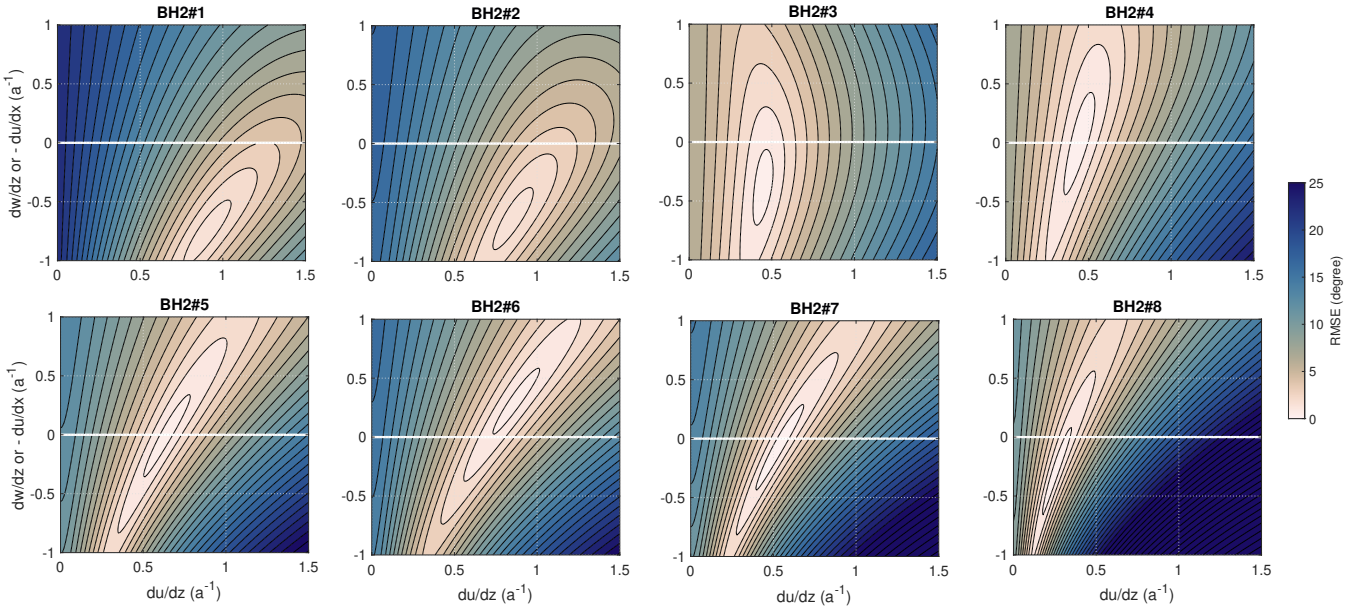

Figure S4: Computed RMSE between observed and modeled tilt evolution following Keller and Blatter (2012) as a function of dw/dz and du/dz for inclinometers BH2#1 to BH2#8. We note that Keller and Blatter (2012) model assume dw/dz=-du/dx from mass conservation and dv/dy=0.

We model the recorded tilt evolution $\theta(t)$ using the analytical formulation proposed by Keller and Blatter (2012) under the hypothesis of constant flow gradient through time. The tilt evolution is a function of du/dz and dw/dz for which we find the best value to fit the data using a simple grid search approach. The value of ϕ_0 is set to $\pi/2$ if the recorded θ go through a minimum (ex: Figure S1, BH2#3) and the value of θ_0 is given by the minimum value of θ. If θ does not go through a minimum (ex: Figure S1, BH2#8), ϕ_0 is set to 0 and θ_0 is given by the initial value of the recorded timeserie. The Root Mean Square Error (RMSE) between model and data are shown for each timeserie in Figures S4 and S5 as a function of du/dz and dw/dz. Note that under the assumption $dv/dy = 0$, $dw/dz = -du/dx$ due to the incompressibility of ice. The resulting tilt curves with the best values of du/dz and dw/dz are shown in Figures S6 and S7. The reconstructed du/dz as a function of depth is shown in Figure S8a and compared with that reconstructed using Eq. (1) in the main manuscript. It shows good agreement between the two approaches except for the two deepest sensors, which are likely influenced by extensive horizontal strain, and BH2#6, which is found to be influenced by compressive horizontal strain. In the case of BH2#6, the Keller and Blatter (2012) model tends to infer positive dw/dz (see Figure S4) because of a decreasing tilt change rate at the end of the time series (see figure S6). However, this change is likely due to a temporal change in the stress field and associated du/dz change (see main manuscript) and the Keller and Blatter (2012) model likely overestimate the mean du/dz here. The temporal variation of strain also likely affect the reconstructed du/dz at other depth making the Keller and Blatter (2012) not appropriate to evaluate du/dz using the whole timeserie. For comparison, we also show du/dz derived from the

Keller and Blatter (2012) model with $dw/dz = 0$, which is closer to the original value using Eq. (1) in the main manuscript and probably more realistic, given that the modeled dw/dz outside the basal layer is very small (see Figure S13). In conclusion, it is likely that compressive/extensive strains play a role only for the two deepest sensors, and that Eq. (1) of the main manuscript is more appropriate elsewhere because of the time-varying strain rate.

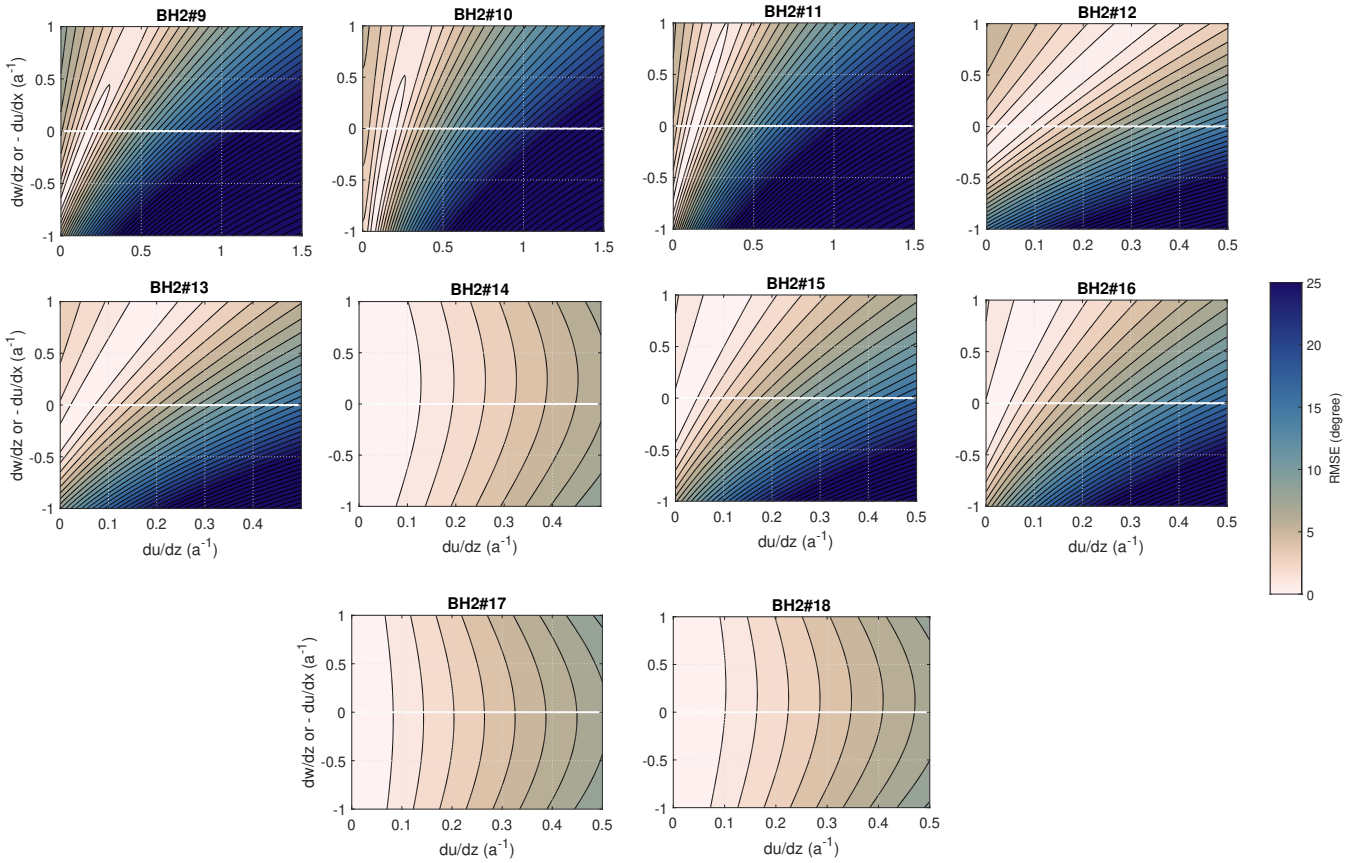

Figure S5: Same as Figure S4 but for inclinometers #9 to #18 of BH2.

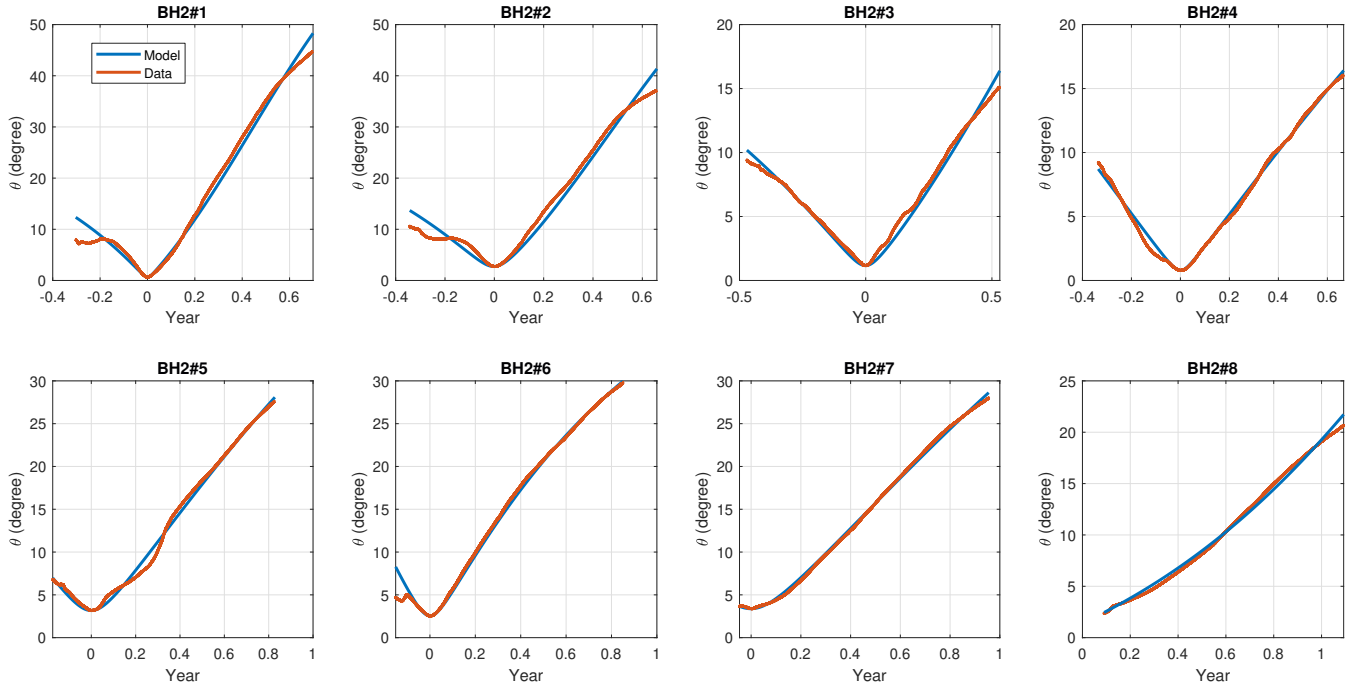

Figure S6: Observed and modeled tilt evolution following Keller and Blatter (2012) for inclinometers BH2#1 to BH2#8.

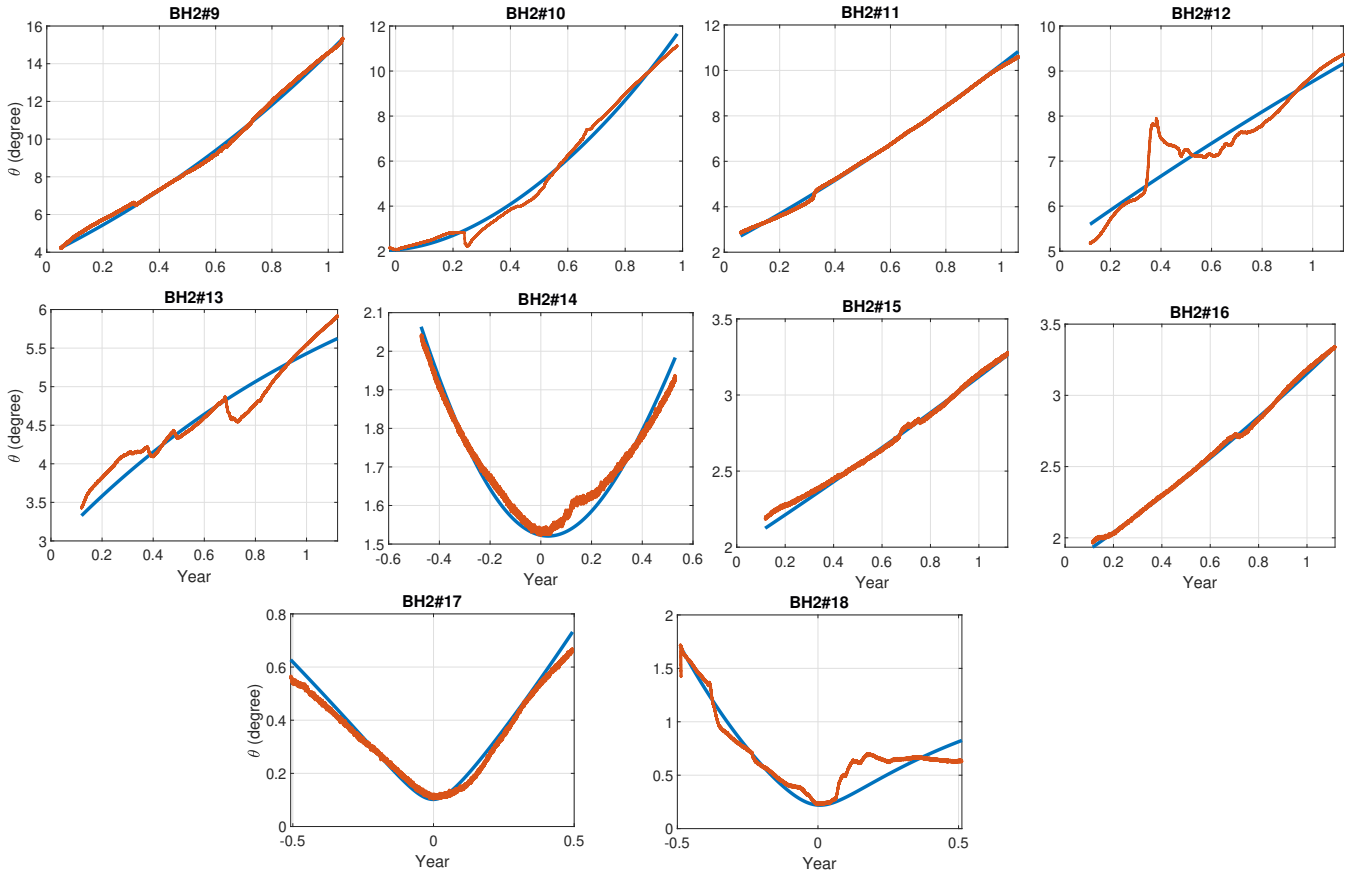

Figure S7: Same as Figure S6 but for inclinometers BH2#9 to BH2#18.

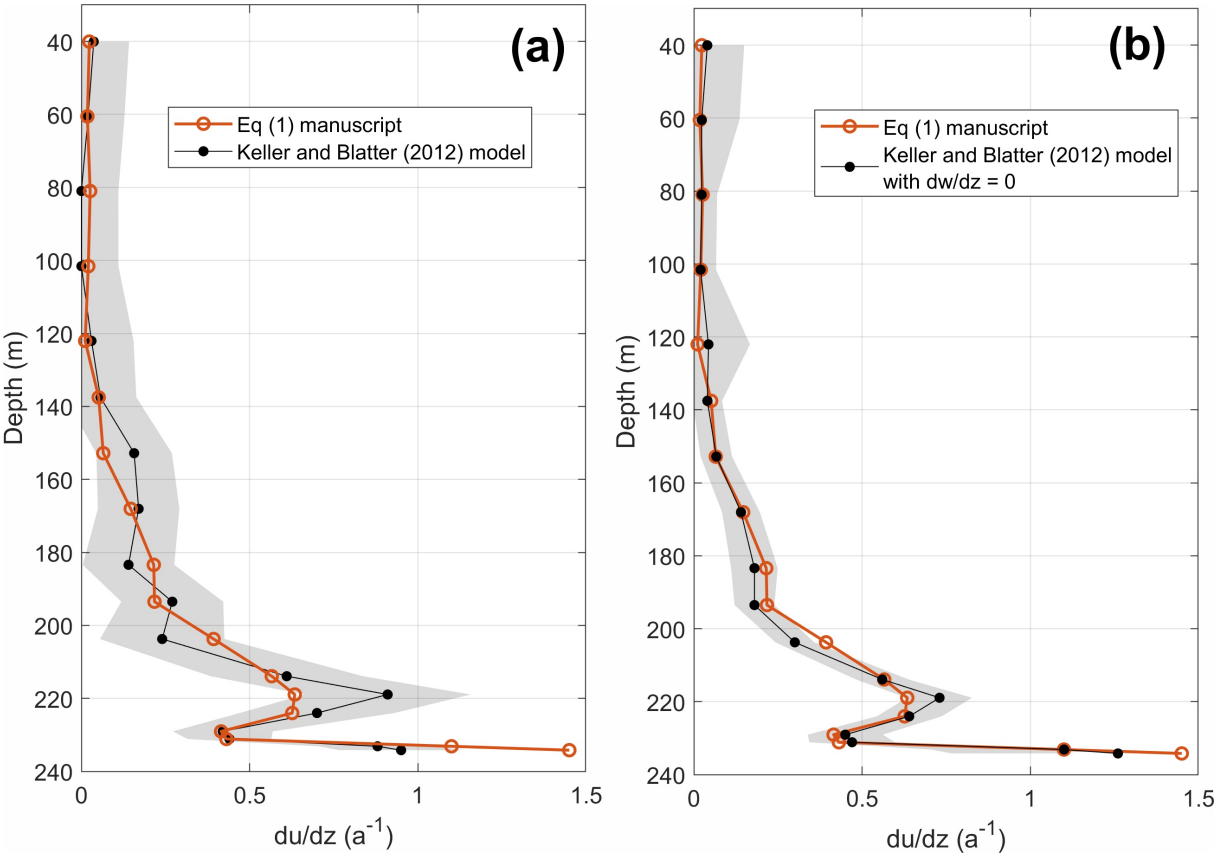

Figure S8: (a) Estimated du/dz using Keller and Blatter (2012) compared to estimated average du/dz using Eq. (1) from the main manuscript (see Figure 2 of the main text). (b) Same but with imposing $dw/dz = 0$ in the Keller and Blatter (2012) model.

S3. Estimation of the error on du/dz and u_d

The deformation is given by:

$$\frac{du}{dz} = \frac{\Delta \tan\theta}{\Delta t}, \tag{S1}$$

and thus the error in du/dz is, by propagation of uncertainties,

$$\epsilon_{du/dz} = \frac{1}{\Delta t}\frac{d\tan\theta}{d\theta}\epsilon_\theta = \frac{1}{\Delta t}(1+\tan^2\theta)\epsilon_\theta, \tag{S2}$$

where Δt is the time period we use to compute du/dz, θ is the tilt and ϵ_θ is the maximum error on evaluating θ. The precision in θ is set by the constructor to 0.01°, such that the error is 0.005°. Since we measure the change over a series of values, the maximum error will be equal to the precision,

$$\epsilon_\theta = 0.01^\circ = 0.00017 \text{ rad.} \tag{S3}$$

Based on our retrieved tilt, we can define two limit angles, $\theta = 0$ and $\theta = \pi/4$, such that the limit error will be

$$\epsilon_0 = \frac{1}{\Delta t}\epsilon_\theta, \ \epsilon_{\pi/4} = 2\epsilon_0. \tag{S4}$$

With this in mind, we can plot the du/dz error map as a function of θ and Δt in Figure S9. The error in the velocity integrated over a thickness Δz can be roughly estimated as

$$\epsilon_u = \epsilon_{du/dz}\Delta z. \tag{S5}$$

We plot two example estimates of the error in u_d in Figure S10. Since it is reasonable to estimate that for most of the thickness the tilt at BH2 is closer to 0 than to 45°, it is likely that our systematic uncertainty on the weekly deformation velocity is not much greater than 2 m a^{-1}.

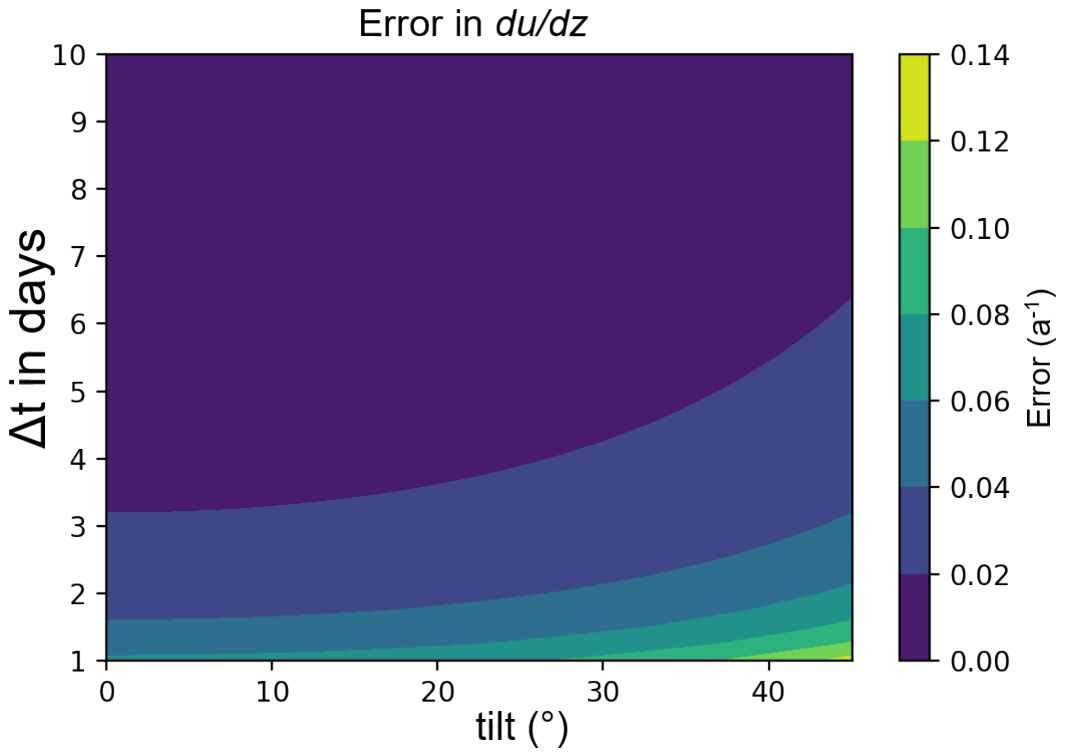

Figure S9: Error in the rate of deformation du/dz. If we take the deformation every few days ($\Delta t \geq 4$, for instance) our systematic uncertainty is almost negligible.

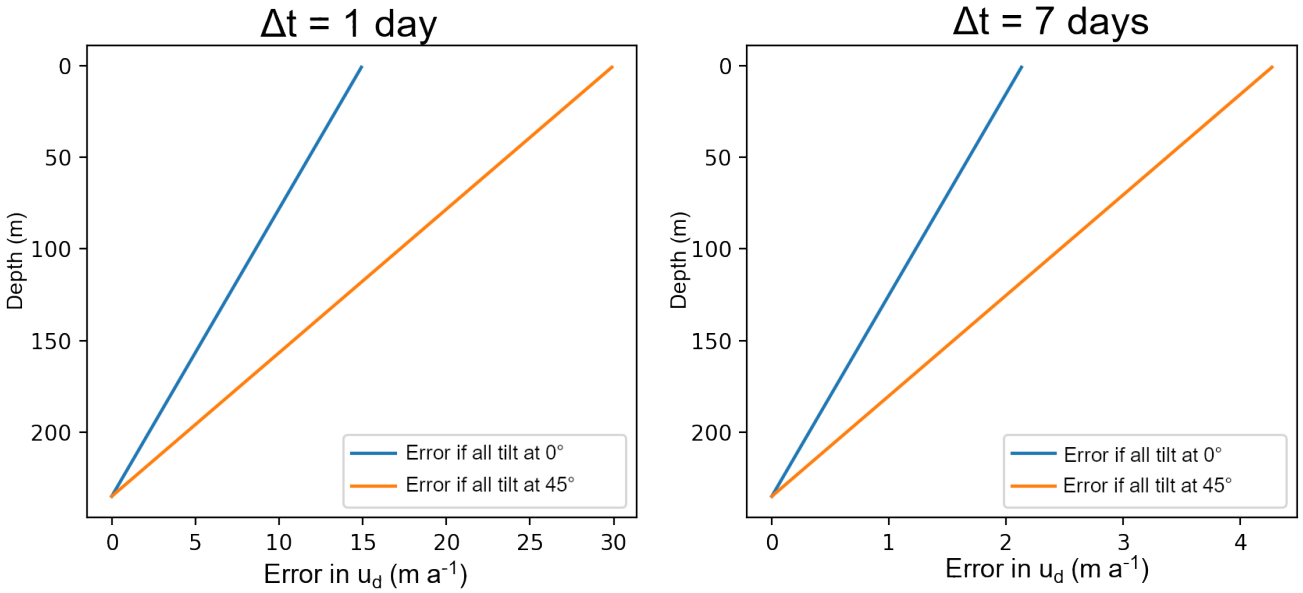

Figure S10: Cumulative systematic uncertainty in the deformation velocity u_d. The real value will be closer to the blue lines, since only a couple tiltmeters are tilting at approximately 45°, and they only cover a few meters.

S4. Residuals between observed and reconstructed daily velocity timeseries

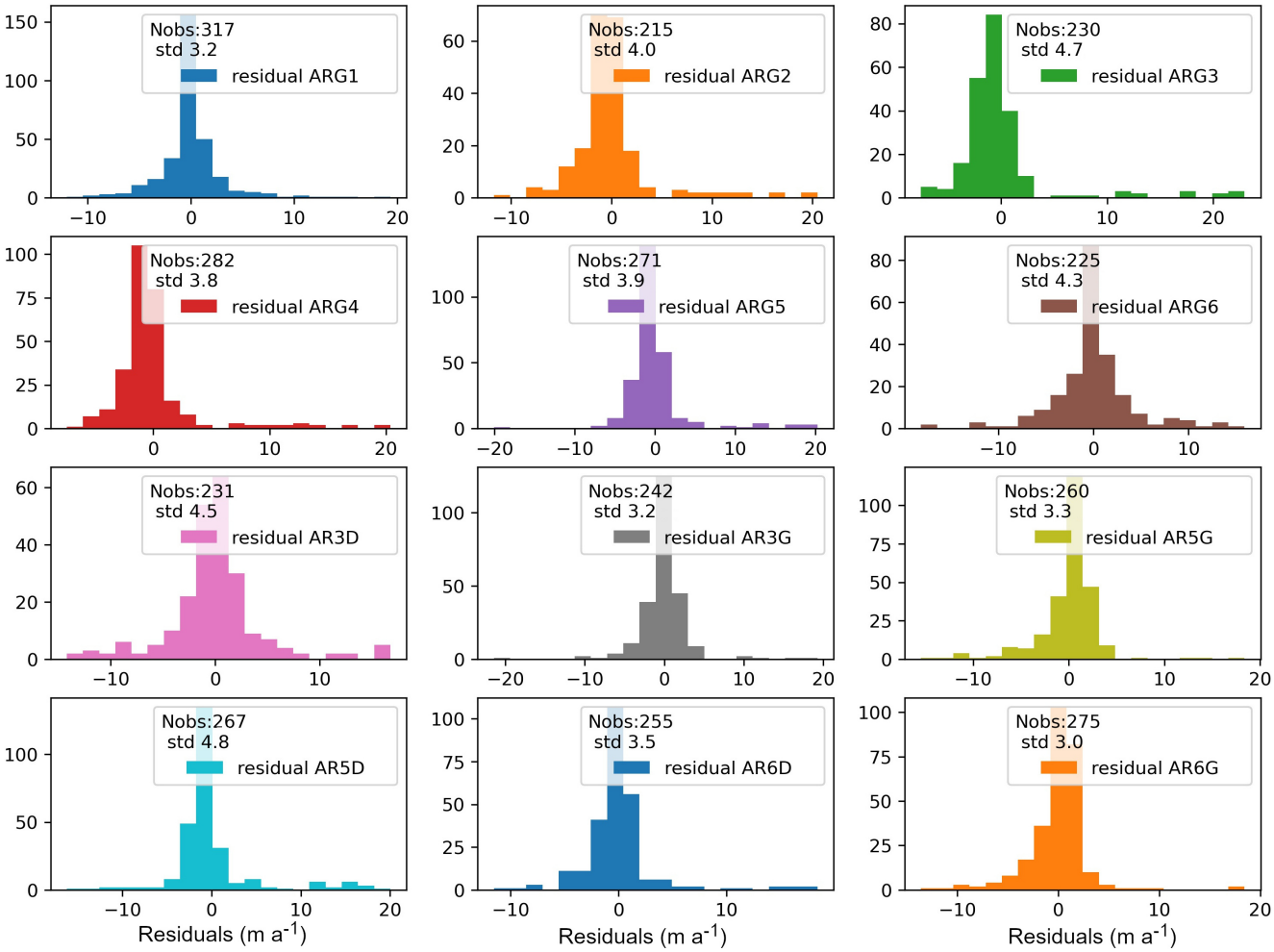

Figure S11: Residuals between observed and reconstructed daily velocity timeseries (m a^{-1}) at each GNSS station using the linear model of Lliboutry (1974).

S5. Modeled stress field and velocity gradient at BH2

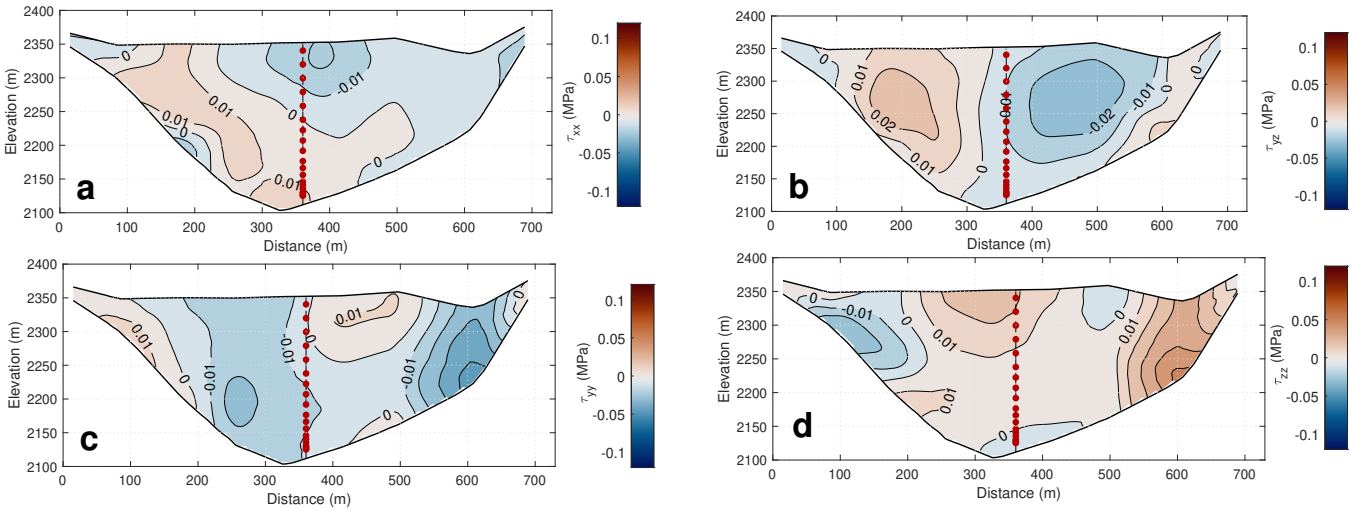

Figure S12: Modeled stress field τ_{xx}, τ_{yy}, τ_{zz} and τ_{yz} along a transversal cross section at BH2 location. The inclinometers from BH2 are shown as red dots

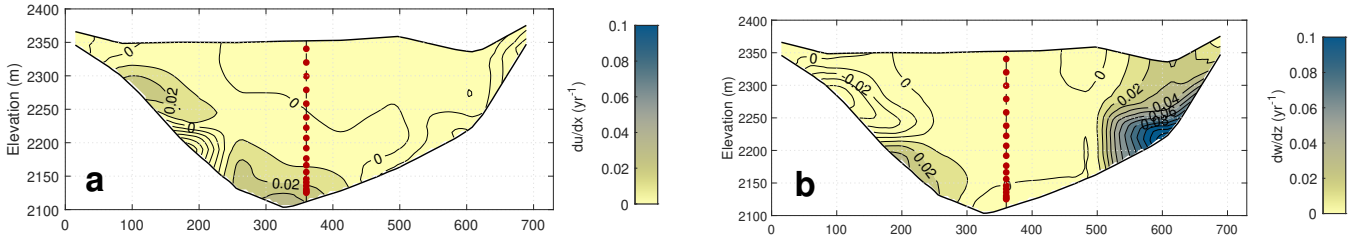

Figure S13: Modeled du/dx (a) and dw/dz (b) along a transversal cross section at BH2 location. The inclinometers from BH2 are shown as red dots.

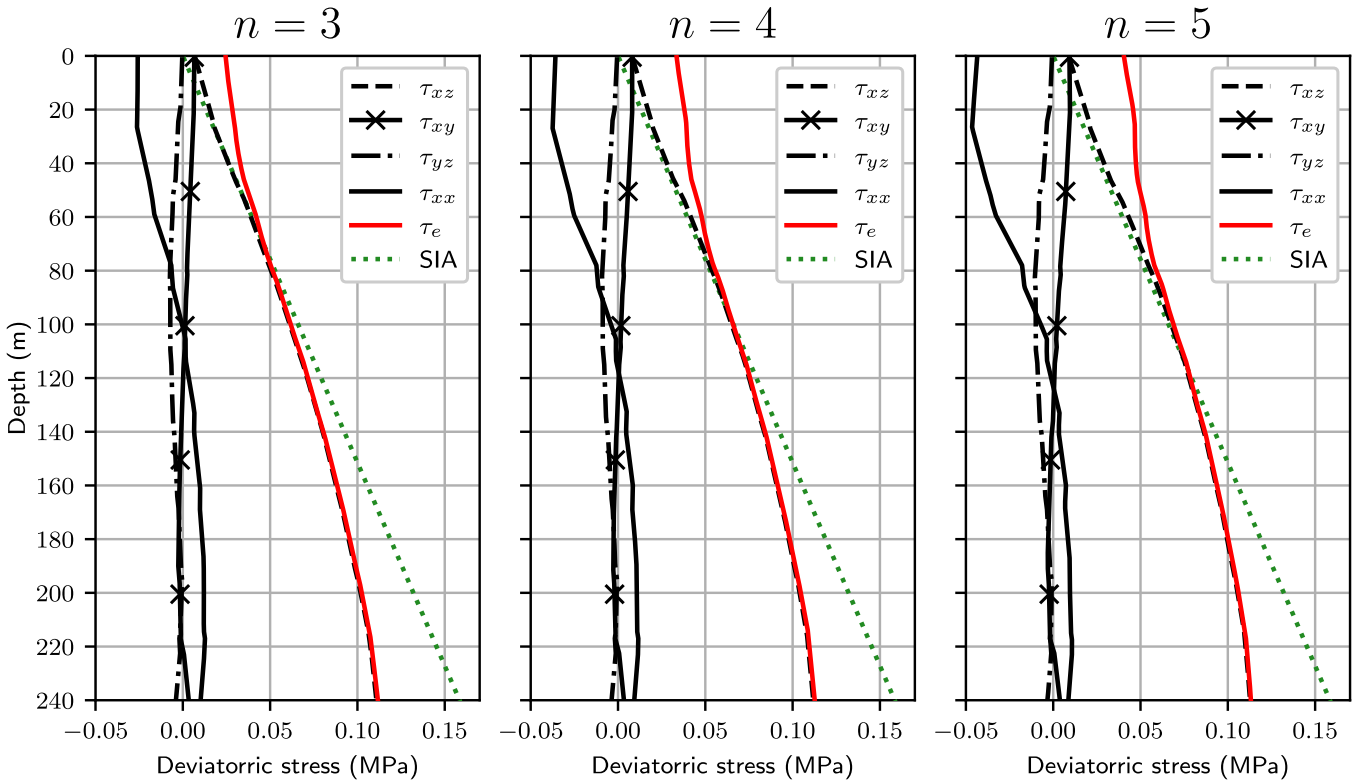

Figure S14: Modeled stress profiles at BH2 for different value of n and uniform creep factor.

S6. Parabolic approximation of Argentière Glacier at BH2 site

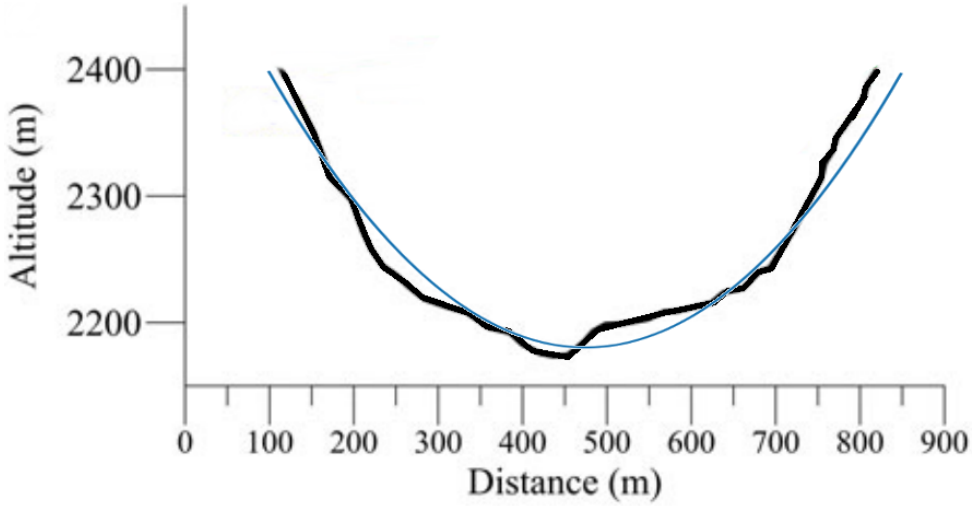

Figure S15: Cross section of Argentière Glacier at BH2 location Vincent et al. (2009) and parabolic approximation of the valley with a half-width to height ratio of 2. Note that the 'Distance' and 'Altitude' axis are not at the same scale.

S7. Temporal variability in du/dz at BH2 site for each sensor

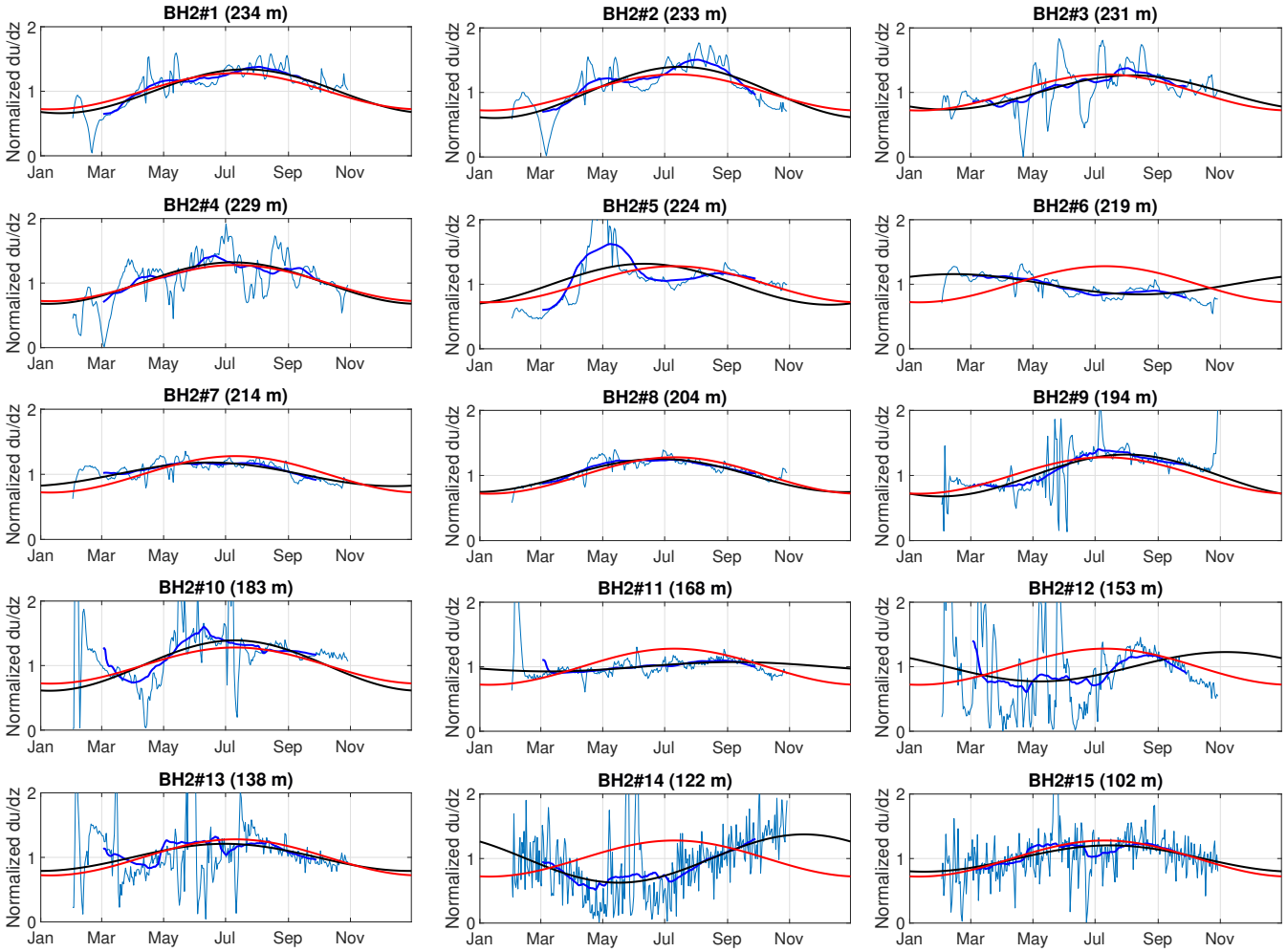

Figure S16: Timeserie of normalized du/dz inferred at each sensor of BH2 (between bedrock and 100m-depth) on daily (blue) and bi-monthly (dark blue) timescale. The black curve shows a 1-year period sinusoidal fit. The red curve is the average sinusoidal fit for all sensors except #6,11,12,14.

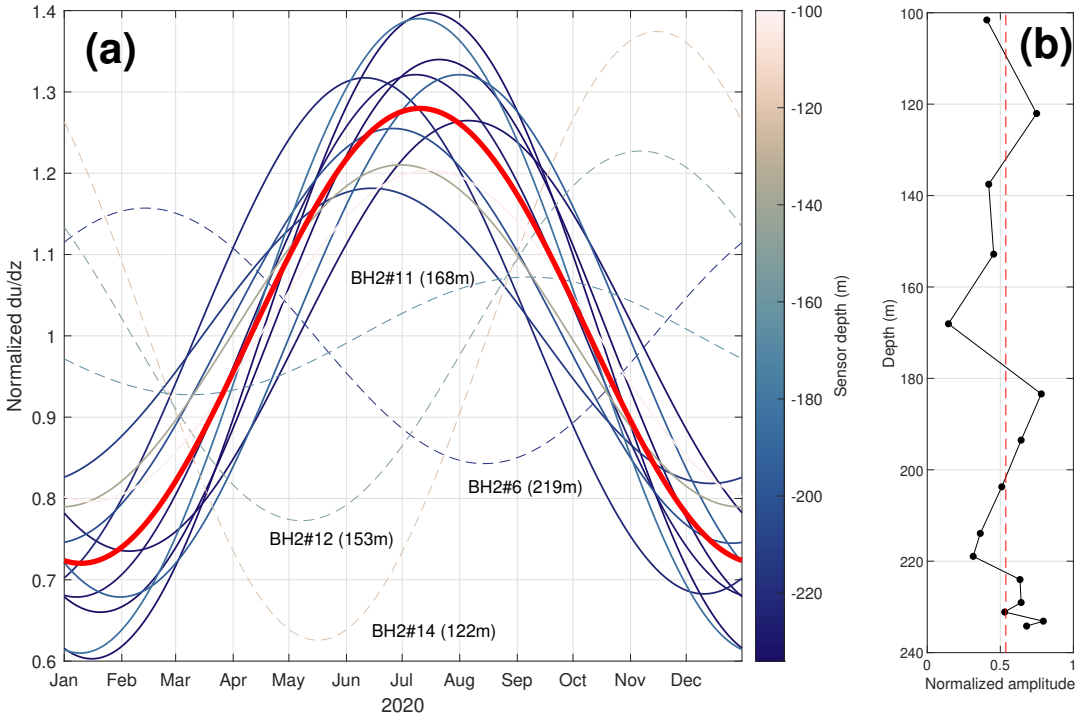

Figure S17: (a) Sinusoidal fits for each sensors (same as in Figure S16). The red curve is the average fit for all sensors except #6,11,12,14 (dashed lines). (b) Amplitude of the sinusoidal fit as a function of depth (black line) and average amplitude (red dashed line).

S8. Influence of the local bed topography on the basal layer

Studies of ice sliding on hard beds show that a boundary layer with important flow gradients develop around the bed bumps (Kamb, 1970; Gudmundsson, 1997a,b) with maximum deformation rates attained a certain distance above the bed, not immediately at the ice-bed interface. In this section, we will compare our observations with an analytically derived deformation rate profile close to the bed following Gudmundsson (1997b) and Gudmundsson et al. (1999).

We simulate the flow around bed bumps using the analytical solution for the two dimensional flow of a linear medium sliding over a sinusoidal bed of low roughness given by Gudmundsson (1997b). We compute the analytical solution using local slope $\varepsilon = 0.5$, glacier thickness $h = 250$ m, and wavenumber $k = 1$, and neglecting regelation. The obtained flow gradient are used to generate one year of synthetic tilt curves, using the forward model of tilt evolution presented in Gudmundsson et al. (1999). We then compute the corresponding apparent deformation rates du/dz using Eq. S1 and compare the results with the du/dz estimated in the main manuscript.

The flow gradients are found to be strongly variable along the flow direction depending on the position relative the to bed roughness (upside or lee side of the bump, see panel (c)). We show that the extension and compression rates are much higher than du/dz and dw/dx in both of the highlighted case (panels (a) and (b)) but of opposite sign. As a result, tilt change is strongly affected by non-shearing stresses, and the inferred apparent du/dz profiles (panel (d)) are different than the actual profiles of du/dz shown in panels (a) and (b). We note that the vertical extension

component dw/dz is not given, since incompressibility with $dv/dy = 0$ makes $dw/dz = -du/dx$. The modeled profile at the upslope part of the bed is qualitatively similar to the observed one, and greatly overestimates the actual du/dz. In conclusion, the observations of the tiltmeters from BH2#1 to BH2#6 cannot be used to directly infer du/dz because they are too much influenced by the compressive or extensive strain-rate associated with the local stress field resulting from sliding over a rough hard-bed.

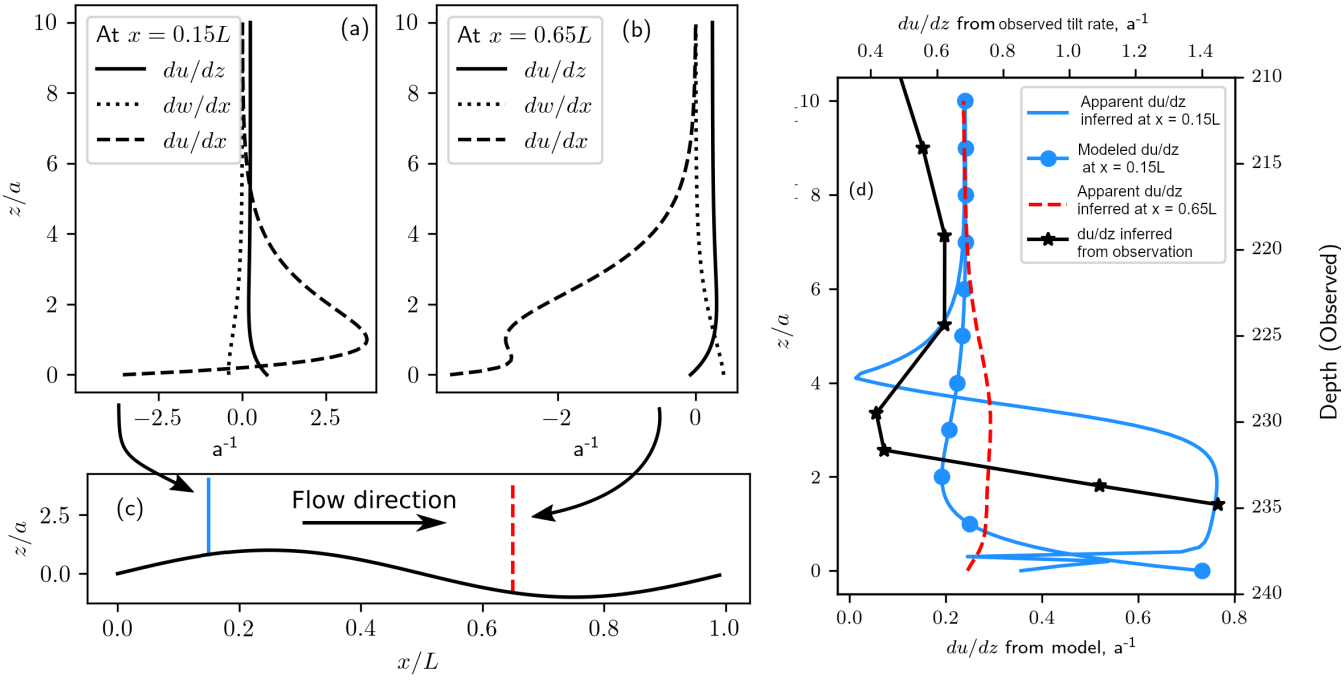

Figure S18: Modeled flow velocity gradient and inferred apparent du/dz from synthetic tilt curves close to a rough bed. Panels (a) and (b) show the analytical vertical profiles of the velocity gradient at two locations of a two-dimensional sinusoidal bed which are given in panel (c). The vertical and horizontal direction in the analytical solution, z and x, are normalized by the bed amplitude a and wavelength L, respectively. Panel (d) compares the apparent inferred du/dz from synthetic tilt curves (continuous blue and dashed red lines), the actual computed du/dz (dotted continuous blue line), and the computed deformation profile in the main manuscript (starred black line, right and top axes). The red and blue colors refer to the position at the bed in panel (c).

References

Gudmundsson, G. H.: Basal-flow characteristics of a non-linear flow sliding frictionless over strongly undulating bedrock, Journal of Glaciology, 43, 80–89, https://doi.org/10.1017/s0022143000002835, 1997a.

Gudmundsson, G. H.: Basal-flow characteristics of a linear medium sliding frictionless over small bedrock undulations, Journal of Glaciology, 43, 71–79, https://doi.org/10.1017/s0022143000002823, 1997b.

Gudmundsson, G. H., Bauder, A., Lüthi, M., Fischer, U. H., and Funk, M.: Estimating rates of basal motion and internal ice deformation from continuous tilt measurements, Annals of Glaciology, 28, 247–252, https://doi.org/10.3189/172756499781821751, 1999.

Kamb, B.: Sliding motion of glaciers: Theory and observation, Reviews of Geophysics, 8, 673–728, https://doi.org/10.1029/RG008i004p00673, 1970.

Keller, A. and Blatter, H.: Measurement of strain-rate components in a glacier with embedded inclinometers, Journal of Glaciology, 58, 692–698, https://doi.org/10.3189/2012JoG11J234, 2012.

Lliboutry, L.: Multivariate Statistical Analysis of Glacier Annual Balances, Journal of Glaciology, 13, 371–392, https://doi.org/10.3189/s0022143000023169, 1974.

Vincent, C., Soruco, A., Six, D., and Meur, E. L.: Glacier thickening and decay analysis from 50 years of glaciological observations performed on Glacier d'Argentière, Mont Blanc area, France, Annals of Glaciology, 50, 73–79, https://doi.org/10.3189/172756409787769500, 2009.